Electronic Supplementary Material (ESI) for Journal of Materials Chemistry B.

Supporting Information

Delivery of Amino Acid Oxidase via Catalytic Nanocapsules to Enable Effective Tumor Inhibition

Qiang Chu, [a,†] Huimin Zhu, [a,†] Bin Liu, [a] Guodong Cao, [b] Chao Fang, [a] Yulian Wu, [b] Xiang Li [a,*] and Gaorong Han [a]

[a.] *State Key Laboratory of Silicon Materials, School of Materials Science and Engineering, Zhejiang University, Hangzhou 310027, P.R. China*

[b.] *Department of Surgery, Second Affiliated Hospital，Zhejiang University School of Medicine，Zhejiang University，Hangzhou, 310000, P. R. China*

† Authors with equal contribution

*Corresponding authors: xiang.li@zju.edu.cn (X. Li)

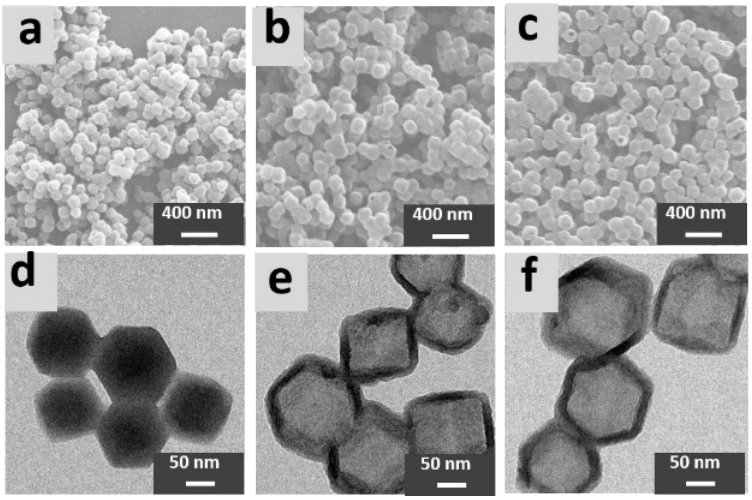

Figure S1. SEM and TEM images of ZIF8 (a, d), hollow TA (b, e) and HFe-TA (c, f) nanoparticles.

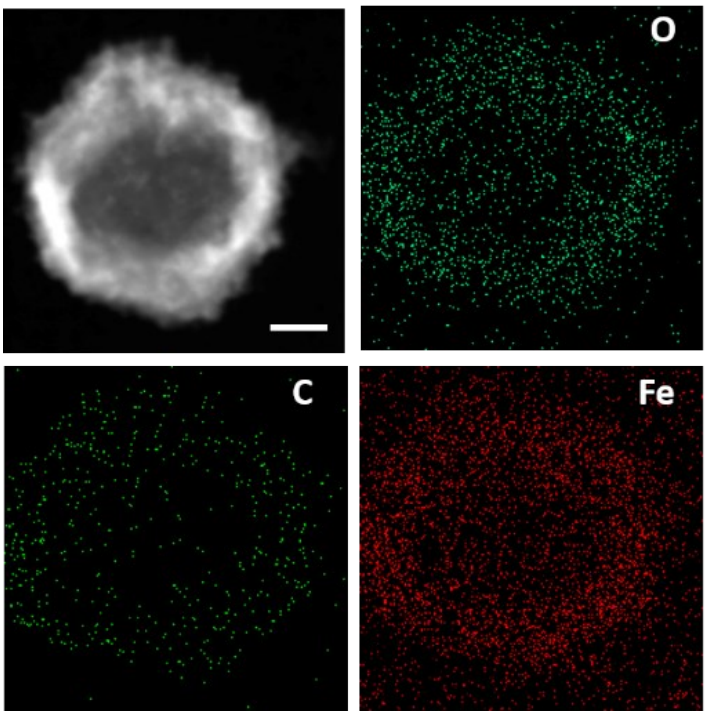

Figure S2. EDS element mapping images of HFe-TA nanoparticles (scale bar: 50 nm).

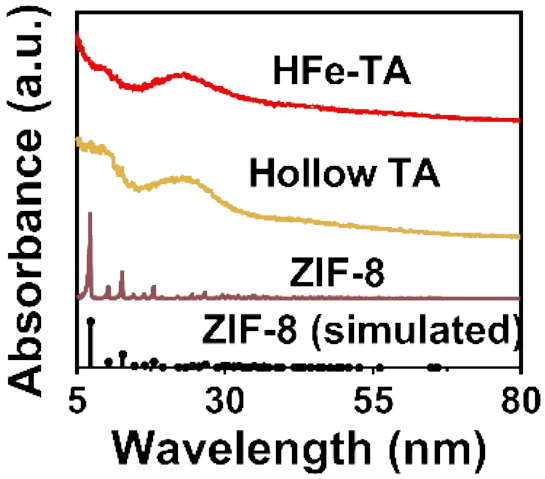

Figure S3. XRD analysis of ZIF8, hollow TA and HFe-TA nanoparticles.

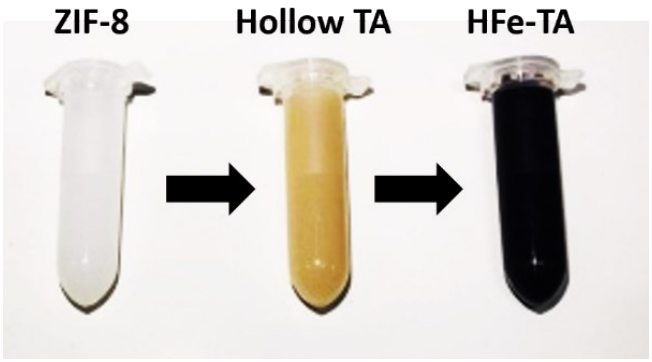

Figure S4. The color of ZIF8, hollow TA and HFe-TA nanoparticles solutions during synthetic process.

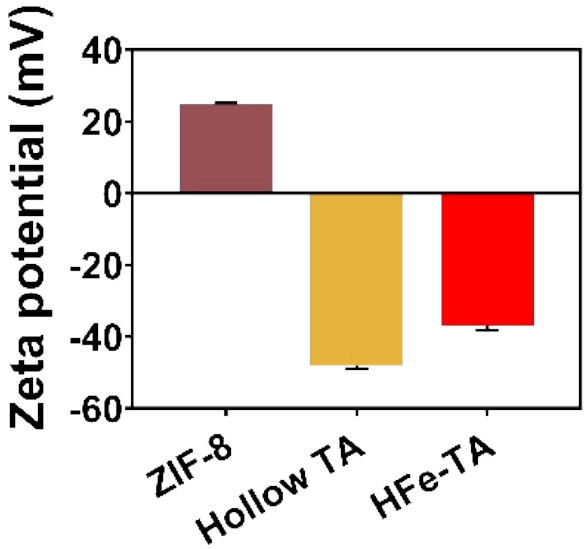

Figure S5. Zeta potentials of ZIF8, hollow TA and HFe-TA nanoparticles.

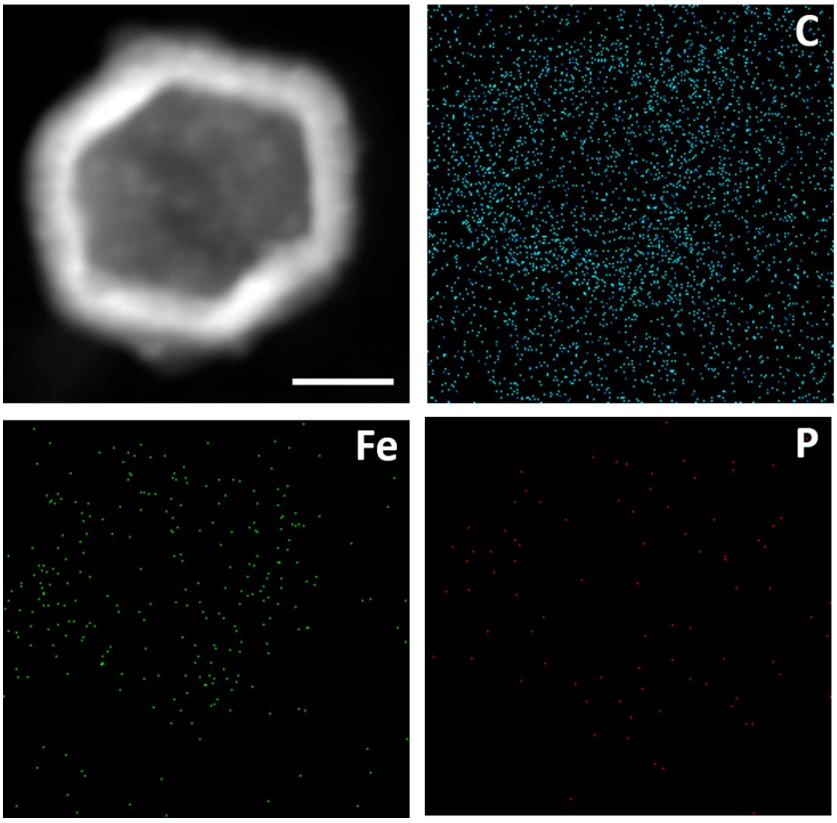

Figure S6. EDS element mapping (scale bar: 50 nm) images of AAO@HFe-TA nanoparticles.

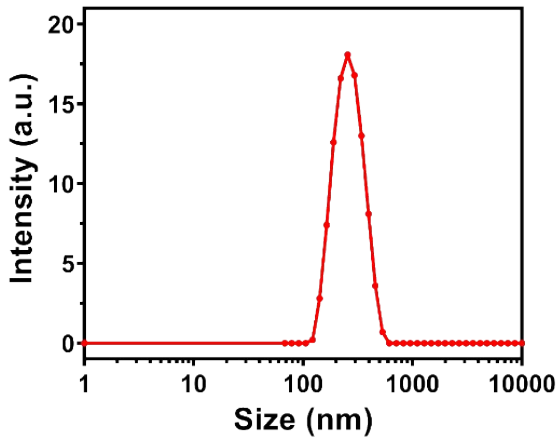

Figure S7. DLS pattern of as-prepared M@AAO@HFe-TA.

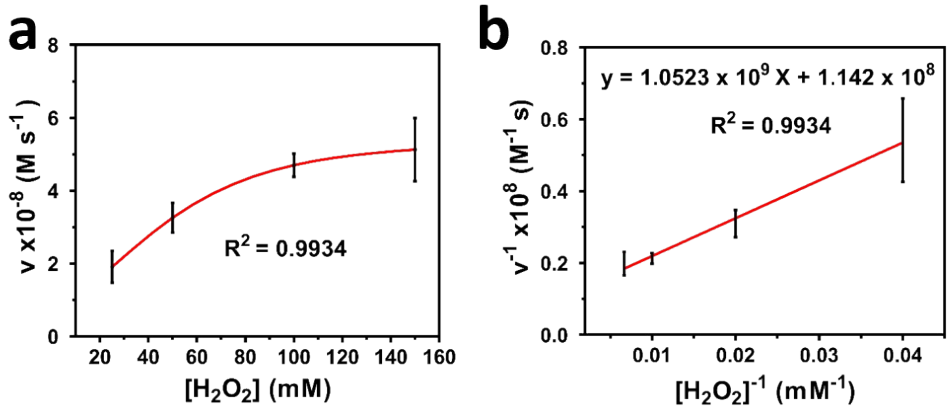

Figure S8. (a)The Michaelis-Menten fitting curves of initial hydroxyl radical generation velocities versus H_2O_2 concentration. (b) The Lineweaver-Burke fitting (double reciprocal) of Michaelis-Menten fitting curve. (Mean values and error bars are defined as mean and s.d. , respectively.)

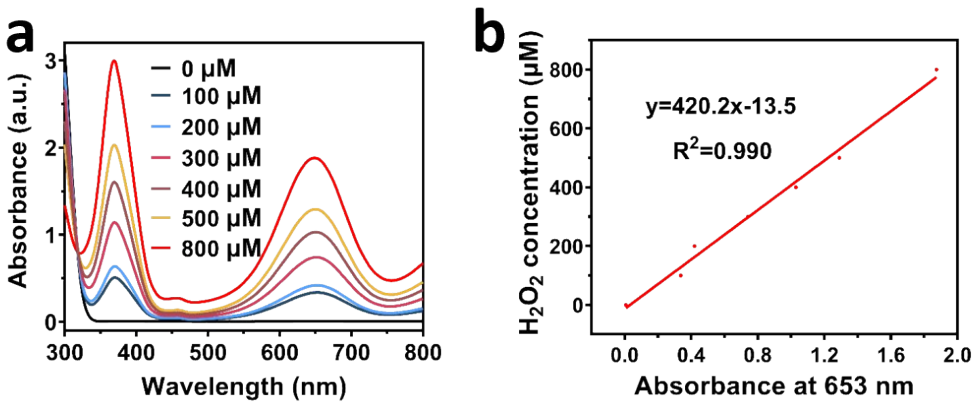

Figure S9. Standard curves of H_2O_2 solution at the peak of 653 nm by TMB method: (a) UV-vis absorbance spectra and (b) plotting curve of of the absorbance at 653 nm.

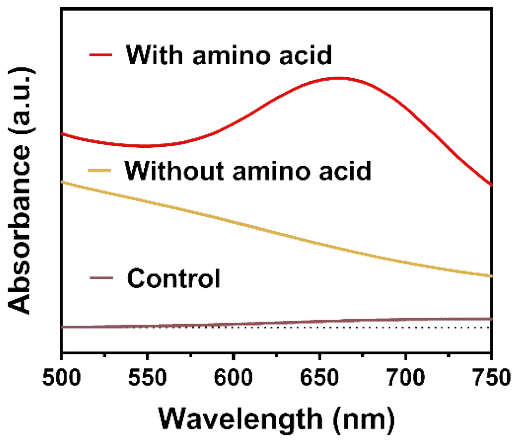

Figure S10. UV-vis absorbance spectra of M@AAO@HFe-TA and TMB solution with or without amino acid.

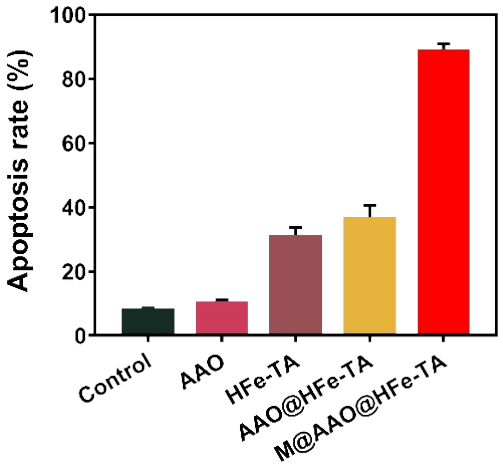

Figure S11. The apoptosis rates of 4T1 cells incbuated with PBS, AAO, HFe-TA, AAO@HFe-TA and M@AAO@HFe-TA analyzed by flow cytometry.

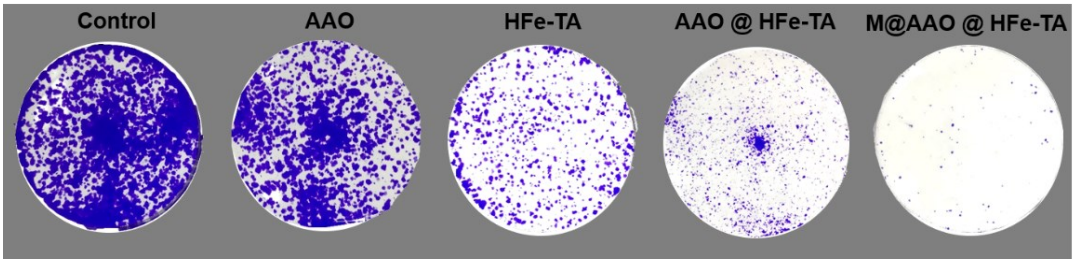

Figure S12. The colony formation of 4T1 cells incubated with PBS, AAO, HFe-TA, AAO@HFe-TA and M@AAO@HFe-TA.

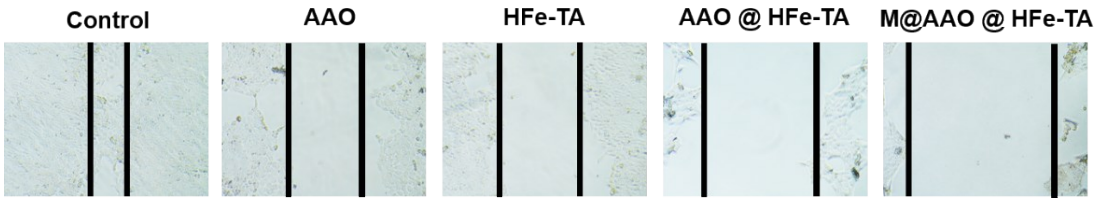

Figure S13. The migration capacity of 4T1 cells incubated with PBS, AAO, HFe-TA, AAO@HFe-TA and M@AAO@HFe-TA.

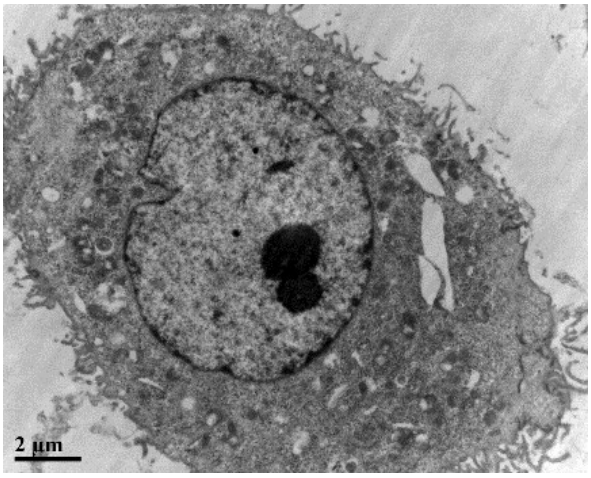

Figure S14. The microrheological characteristics of untreated 4T1 cells

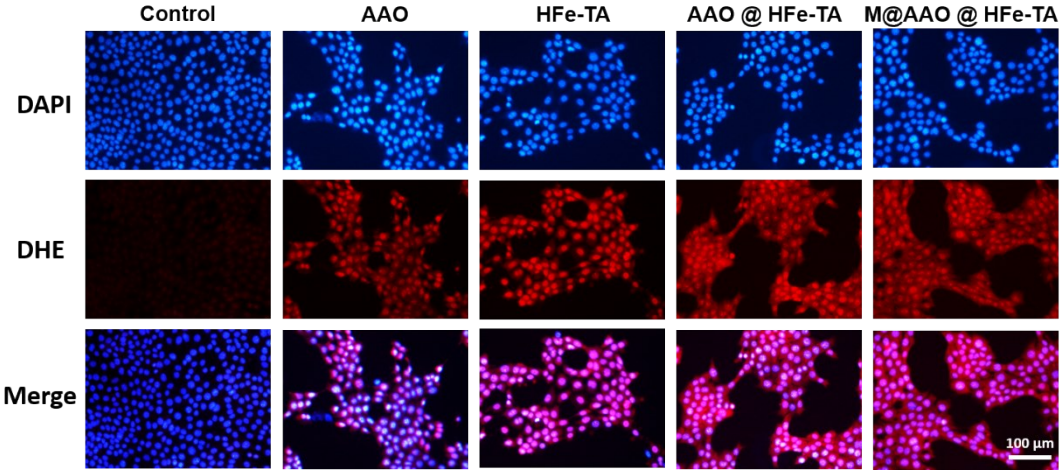

Figure S15. DHE (red fluorescence) and DAPI (green fluorescence) staining for the generation of $\bullet O_2^-$ in 4T1 cells incubated with PBS, AAO, HFe-TA, AAO@HFe-TA and M@AAO@HFe-TA.

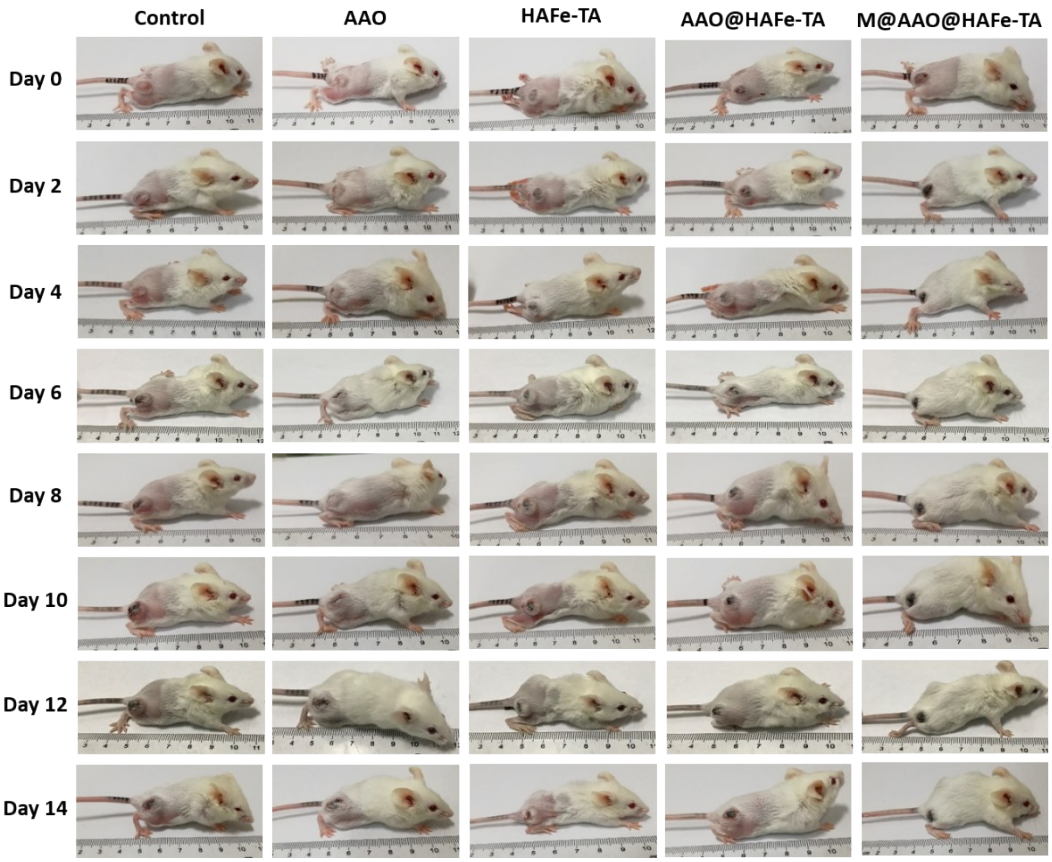

Figure S16. Images of 4T1 tumor-bearing Balb/c mice of 5 groups on every 2-day in 14 days.

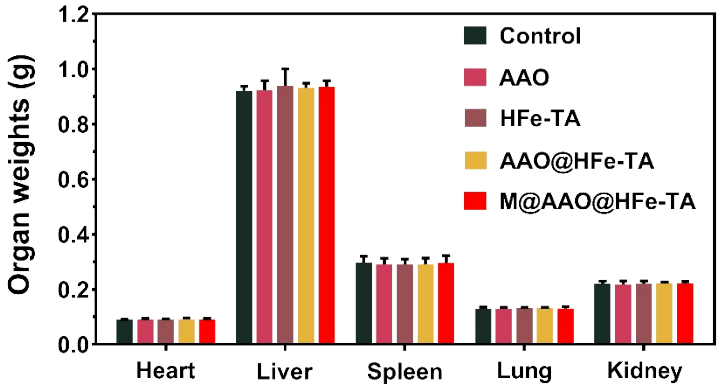

Figure S17. The average weight of major organs in PBS, AAO, HFe-TA, AAO@HFe-TA and M@AAO@HFe-TA treated 4T1 tumor-bearing Balb/c mice.

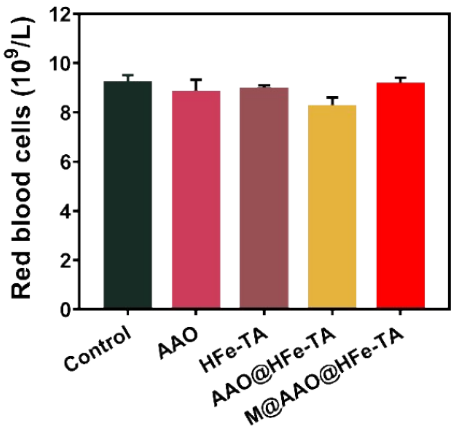

Figure S18. The number of red blood cells in PBS, AAO, HFe-TA, AAO@HFe-TA and M@AAO@HFe-TA treated 4T1 tumor-bearing Balb/c mice.

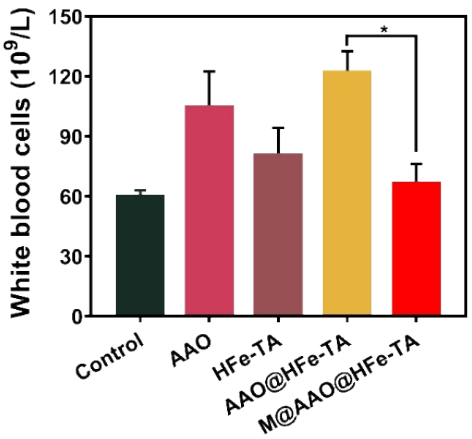

Figure S19. The number of white blood cells in PBS, AAO, HFe-TA, AAO@HFe-TA and M@AAO@HFe-TA treated 4T1 tumor-bearing Balb/c mice.

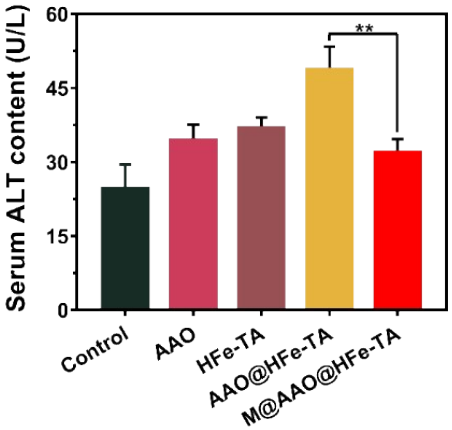

Figure S20. Serum ALT contents in PBS, AAO, HFe-TA, AAO@HFe-TA and M@AAO@HFe-TA treated 4T1 tumor-bearing Balb/c mice.

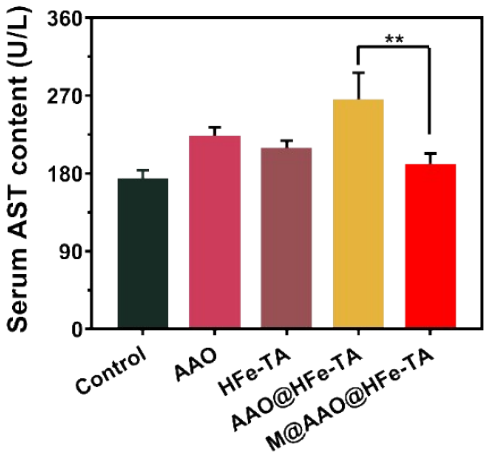

Figure S21. Serum AST contents in PBS, AAO, HFe-TA, AAO@HFe-TA and M@AAO@HFe-TA treated 4T1 tumor-bearing Balb/c mice.